J. of Fire Prot. Engr., 7 (4), 1995, pp 107-124

COMPUTER AIDED INFRARED IMAGERY FOR FABRIC SURFACE TEMPERATURE FIELDS UNDER SIMULATED CIGARETTE EXPOSURE

Sanjeev Gandhi and Steven M. Spivak
Department of Fire Protection Engineering
University of Maryland
College Park, MD
and
Behnam Pourdeyhimi
School of Textile and Fiber Engineering
Georgia Institute of Technology
Atlanta, GA

SUMMARY

This paper, the first of two parts, describes a technique of measuring dynamic temperature fields on thin, porous textile materials when exposed to a low energy, localized heat source. A methodology is outlined for studying the smoldering process via measurement of surface temperature profiles using calibrated infrared (IR) thermography, a non-intrusive technique for the measurement and analysis of a material's surface temperature. This paper outlines the essential elements necessary for proper use of IR thermography and provides a summary of thermal radiation theory, combined with computer enhancement of the thermographs.

An advanced thermal imaging system couples non-contact infrared thermography with personal computer-based image processing routines for the measurement of real-time temperature and heat flow patterns. The instrumental set-up described here facilitates instantaneous scanning, detection, and depiction of temperature variations and isotherms. Such a system allows continuous, real-time or post-experiment processing and analysis of thermal images in color or gray scale, via digitization followed by image enhancement. A typical protocol of computational techniques and image analysis steps are described for obtaining thermographic data and to analyze growth of conditions leading to smolder initiation, typically in a cellulosic fabric. This methodology can be employed for dynamic measurement of temperature and heat flow though porous materials such as upholstery cover fabric, insulation material, protective clothing, etc.

INTRODUCTION

IR thermography, a non-contact temperature measurement technique, is capable of producing analog and/or digital radiometric data (normally presented in the form of an image) by mapping infrared radiation for a given temperature range. The data are often calibrated to represent absolute temperature and are mapped to an image where gray scales are proportional to temperature. Because IR thermography determines the radiant energy emitted by the target, it allows dynamic changes in the thermal characteristics to be observed and recorded. The system can also provide time dependent representation of temperature distribution in a defined target field. Standard image processing and analysis techniques can be employed to process, enhance, and extract quantitative thermal data from the IR signals or the IR images.

In obtaining quantitative data, three steps are involved. Image acquisition refers to the digitization of the analog signals produced by the camera. Image processing refers to means of transforming a digital image where extraction of useful data becomes easier. (Filtering noise is one such process.) Image analysis is the last step where the extraction of numerical data pertinent to user's application, such as temperature data from a thermal scene, is accomplished.

Image processing and analysis techniques are employed in myriad scientific and industrial applications such as biomedical and radiological diagnostics, nuclear physics, remote sensing, microelectronics, robot-

ics, machine vision and automation, and forensic sciences[1,2]. By coupling IR thermography with image analysis, this technique has proven successful for detection of hot spots, heat losses, and cracks in materials and composite structures[3,4].

In many situations, one is interested in analyzing the thermal changes in an object (or a scene). IR thermography provides a spatial distribution of temperature and related properties without the physical contact necessary when using thermocouples and thermistors. The simplicity of thermocouples makes them an obvious choice in many applications. However, contact-based thermometric measurements are prone to several types of errors including thermal expansion and structural inhomogeneity due to metallurgical changes. The various error types associated with different measurement techniques are described in detail by Nicholas and White[5]. Unlike contact-based instrumentation that gives a point measurement, the thermography process is broad field and does not affect the measurement itself. Also, a rapid response time on the order of 2 microseconds achieved through infrared temperature sensors provide real-time profiles of a thermally dynamic system[6]. The advantages of an IR-based temperature measurement system are specially useful in physically inaccessible, moving or rotating, harsh, and corrosive environments[6,7].

Originally developed as an air-borne system for military and intelligence purposes[8], thermal imaging systems were given the acronym FLIR for Forward Looking Infrared. However, any fast-framing thermal imaging system that converts IR radiation to a visible spectrum is now referred to as FLIR[8]. Over the past three decades, thermal imaging systems have found applications far beyond weapon sight systems. With simultaneous developments in digital electronics, computer technology, and infrared detectors, IR systems are now being used for numerous research and industrial applications[9]. IR thermography has become a major diagnostic tool for nondestructive testing and evaluation in building evaluation[10,11], aerospace[9], microelectronics[12], and medical research[13]. In fire research, radiation measurement using thermography have been made for evaluating protective clothing performance[14] and analysis of large-scale kerosene pool flames[15]. Saito and Arakawa employed IR imaging for measurement of temperature in fire induced flow along a vertical corner wall[16].

In this paper, a methodology is described for the measurement of transient temperature distributions due to smoldering ignition of a porous textile material. The term ignition throughout the text refers to smoldering ignition. Smoldering combustion of cellulosic materials such as cotton and rayon textile cover fabrics plays a major role in the initiation of furniture and bedding fires. The ignition commonly results from exposure to a low energy, moving heat source such as the fire cone of a lit cigarette. Smoldering ignition in cellulosic materials has not been studied in detail owing to many variables. The complexity of the smoldering process stems from the variety of physical and chemical properties of both the substrate and the ignition source, the ambient oxygen concentration, and their interaction. In response to the imposed heat flux distribution, the fabric surface temperature increases to its degradation point, resulting in the formation of cellulosic char. An exothermic reaction involving char oxidation releases sufficient energy to cause further pyrolysis of the material and self-propagating smolder, provided sufficient ambient oxygen is available. The measurement of a two-dimensional, dynamic temperature field in the exposed material is important for predicting the growth of conditions leading to smoldering ignition.

The objectives of this experimental study are twofold: (a) to employ infrared thermography and digital image processing

techniques for improved measurement of a two-dimensional temperature field and heat flow patterns on the surface of a thin, porous textile fabric when exposed to a low energy, localized heat source; and (b) to use these refined measurements to gain better insight into the physics involved in smoldering. The measurement of dynamic temperature field on the surface of fabric is particularly useful since essentially all smoldering fires start through the cover fabric before involving the entire substrate. To this end, an infrared radiation measurement device is used for temperature measurements. The instrumental arrangement is predicated on the accuracy and repeatability of measurements accorded by infrared devices. In this paper, the essential elements constituting infrared thermography are reviewed, and a methodology is outlined for extracting quantitative thermal data using image-processing techniques. Specific image-processing routines were developed to facilitate derivation and depiction of temperature gradients from thermal images. Instrumentation is used for the measurement of a diverse temperature field on the top surface of a porous textile material due to a radiant heat source simulating a lit cigarette. Preliminary experiments describe a simple case where single layers of upholstery cover fabrics were used for the smoldering study. Duck fabrics chosen for this study have the same chemical composition with only slight differences in their physical properties. The premise is that if IR thermography can reveal relative differences in temperature patterns upon two fabrics of similar construction, it is very likely to elucidate differences between materials with significantly different characteristics.

Infrared Radiation Physics

All objects emit IR radiation, which unlike the visible spectrum (0.40 μm to 0.75 μm), occupies a much broader bandwidth extending up to 1000 μm. Infrared emission from a surface, a form of electromagnetic radiation, results from molecular and atomic agitation due to internal energy of the material. The magnitude of internal agitation is directly linked to the material's temperature. Consequently, temperature of an object is a function of its radiant energy, its emittance, and the ambient thermal conditions[17-19]. This relationship between the radiant energy (W_λ) and the temperature (T, K) at a given wavelength (λ) is established by Planck's Law:

$$W_\lambda = \frac{\varepsilon(\lambda) C_1 \lambda^{-5}}{\pi e^{c_2/\lambda T} - 1} \qquad (1)$$

where $\varepsilon(\lambda)$ is the object's radiating efficiency referred to as its emissivity, and $C_1 = 3.74 \times 10^{-12}$ W•cm^2 and $C_2 = 1.44$ cm•K are constants.

Thermal imaging systems do not measure temperature directly. The emitted energy scaled to the target emissivity yields information about target temperature. If the target is a blackbody, an ideal radiator with unit emissivity, integration of the above expression (Equation 1) over a specific bandwidth determines the total radiant power.

$$E_b = \frac{1}{\pi} \int_{\lambda_1}^{\lambda_2} \frac{\varepsilon(\lambda) C_1 \lambda^{-5}}{e^{c_2/\lambda T} - 1} \qquad (2)$$

Summation of total radiant flux over a broad bandwidth (when λ_1 and λ_2 span over 50 percent of the total radiated power) is given by an approximate solution. This solution, known as Stefan-Boltzmann law, is a fourth order parabola given as:

$$E_b = A\varepsilon \cdot \sigma \cdot T^4 \qquad (3)$$

where $\sigma = 5.67 \times 10^{-8}$ W/m^2•K^4, the Stefan-Boltzmann constant.

The magnitude of the emitted radiation, a measure of body temperature, depends on the surface property known as emissivity (ε). Emissivity, which is the ratio of radi-

ant flux from a real surface to the flux emanating from a blackbody having the same temperature, is measured on a scale of 0 to 1. The emissivity of an object is a function of its temperature, wavelength, and the direction of measurement relative to the surface. For any given material, total emissivity is often measured normal to its surface and integrated over all wavelengths. Total emissivity is the ratio of the radiant energy emitted by the material (at temperature T) and the energy radiated from a blackbody at the same temperature, *i.e.*, a measure of how efficiently a body emits radiant energy. For an opaque body ($\tau=0$), emissivity can be determined indirectly through its reflectance ($\varepsilon+\tau+\rho=1$) and thus $\varepsilon=1-\rho$.

Various methods for direct measurement of surface emissivity using blackbody and specimen temperature calibration are discussed in the literature[20,21]. For completeness, two methods are discussed below. The first is a simple method where the spectral emissivity of a surface is measured using a calibrated thermometer such as a thermocouple. The emissivity setting on the radiation instrument is adjusted to derive a temperature reading that matches that of the thermocouple. Another popular approach calibrates the emissivity by using a blackbody ($\varepsilon=1$) at exactly the same temperature as the object. The emissivity setting on the instrument is then corrected so that object temperature matches the blackbody (reference) temperature.

Note that for accurate measurement of surface emissivity, the emittance from the object should be its own radiation. However, the radiation from an object can be affected by the material reflectance (ρ) which is high for materials with low emissivity. In such a case, part of the energy which is radiated from the surrounding objects gets reflected from the material surface. It is therefore difficult to distinguish between the reflected and emitted components. For an opaque object ($\tau=0$), the error induced by body reflectance is negligible when the surroundings are at a much lower temperature compared to that of the object. The surface emission is then a function of the object temperature.

Infrared Thermography

As noted earlier, IR thermography refers to the technique of producing analog and/or digital radiometric data in the form of a black-and-white image where image gray scales are proportional to temperature. The radiance distribution in the transformed image is a time-based function of the spatial irradiance from the object.

An IR imaging device converts the incident IR radiation to a video signal through its optical system that collects, filters, and focuses radiation onto an array of detector elements that allow a spectrum of point measurements. The detector array size depends on the instrument hardware and the optical system for focusing emitted radiation onto the sensor. For example, a typical state-of-the-art IR camera can provide 256x256 and up to 512x512 point measurements using a mosaic of multi-element detectors.

There are the two major classes of IR detectors: thermal and photon detectors. The photon type detectors respond much faster compared to the former[19,22]. Also known as quantum detector, a photon detector is more sensitive and its output for a specific bandwidth depends on the number of energy photons absorbed. Typical IR systems utilize photosensitive elements such as indium antimony (InSb) and mercury cadmium telluride (HgCdTe) detectors.

An important consideration for potential error in IR thermography involves attenuation of irradiance that occurs due to the intervening environment between the object and the sensor. The attenuation of IR energy emitted from a material surface causes a systematic error in the measurement. The perturbation is due to absorption of radiation by the atmospheric gases and scattering by the particles in the air.

Atmospheric absorption of radiant energy due to gases such as CO_2, O_2 and H_2O is, however, minimal for certain spectral windows. Most commercial IR scanning instruments are designed to operate in the 3-5 μm and 8-14 μm spectral region for least atmospheric attenuation[7]. This is achieved by selecting a photon detector that is sensitive to such wavelength intervals[21,22].

Figure 1 delineates the thermal radiation exchange between an object and the sensor elements of the IR detection system. The output signal from this system, a function of net emittance (E_n) detected by the sensors is given by total radiant flux (E_O) emanating from the object surface of temperature T_O and radiation from the sensor (E_S) due to its temperature T_S, as defined by Stefan's law (Equation 3).

$$E_n = \varepsilon_O \varepsilon_S \sigma (T_O^4 - T_S^4) \quad (4)$$

The above equation forms the quantitative model for the net thermal flux exchange between the object and the sensor which is indicative of target surface temperature. For any given IR system and a selected wavelength band, *e.g.*, 3-5 μm, the output signal $I(T_o)$ is defined by:

$$I(T_O) = \int_3^5 R_{(\lambda)} E_{n_{(\lambda,T_o)}} d\lambda \quad (5)$$

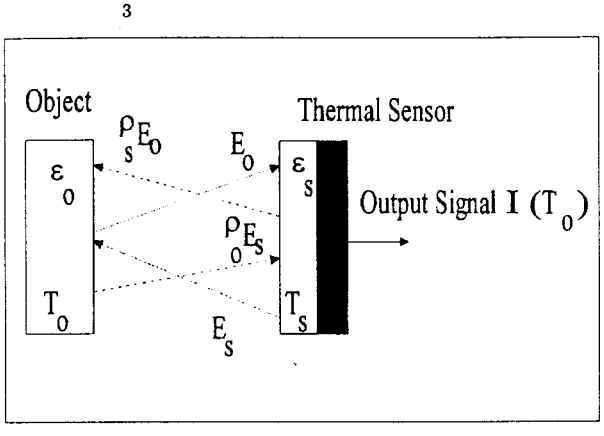

Figure 1. The Output Signal $I(T_o)$ as a Function of Thermal Radiation Exchange between Object and the Detecting Sensor.

where E_n is the net IR radiation received by detector elements of responsivity factor $R(\lambda)$.

Electrical output voltage is amplified and processed for video display in real time, updated at a frame rate comparable to that of television (normally between 20 and 30 frames per second). Thermal images of the scene can be recorded continuously on video cassette or directly in digital form.

Digital Image Processing

To obtain an IR image for the purposes of radiometric measurements requires a sequence of steps. As indicated earlier, the gray scales in an image displayed by IR cameras are related to the object's temperature. These images, however, need to be calibrated and the signal-to-noise ratio needs to be improved prior to the extraction of radiometric data. Most IR cameras output calibrated radiometric data through serial and/or parallel ports, where they can be sampled by a computer. However, the transfer rates are not sufficiently high to allow filed and continuous data acquisition and measurement, but the images can be easily stored and analyzed later. The video images are stored in an analog form and need to be digitized before any measurements are possible. This is accomplished through a frame grabber where the on-board analog to digital converters transform the incoming video signal to a digital form that can be stored and analyzed. The spatial resolution of most frame grabbers exceed that of the IR detectors. The camera used in this study was a Hughes 7300 Probeye IR camera that operates in the 3-5 μm range and provides a spatial resolution of 256x200. The frame grabber employed was a Coreco imaging card. Programs were developed for automatic timed capture and storage of images, with enhanced resolution of 512x486 pixels.

A pixel is the smallest picture element. The number of pixels in the image defines

the spatial resolution of the image. The numeric value assigned to each pixel corresponds to the average brightness of the image area subtended by a pixel in the thermal image and is directly proportional to irradiance from the corresponding point in the thermal scene. A low numeric pixel value is therefore attributive of lower radiation intensity in the original scene, *i.e.*, a pixel value represents the amplitude of the image at that point. The range of values possible for each pixel depend on the memory used up by each pixel. In our system, one byte (8 bits) is used to represent 256 gray scales.

A digital image consisting of a matrix of NxN pixels often needs to be transformed to remove noise and to convert it to a more amenable form for analysis. The procedures employed fall under the heading of image processing (see Figure 2). Collectively, these operations facilitate the task of data extraction. Several image processing algorithms applied for a diverse range of applications are discussed in literature[23-34]. Typical image processing routines that were applied for improving signal to noise ratio are described here as follows.

Presence of noise is a common problem that degrades image quality and subsequently the validity of data based on a corrupt image. There are a variety of "noise"

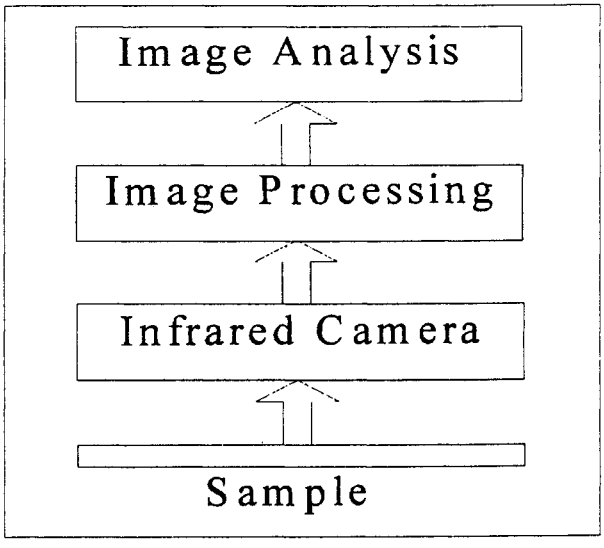

Figure 2. The Principal Steps in Infrared Thermal Imaging System.

types present in an IR image induced from various sources such as IR/video camera, image transmission, digitization, drift, and motion blur, etc. Image noise can be either periodic or stochastic; a very common example of the latter being "snow" on a TV screen. Image noise is usually represented by pixels with much higher gray levels. Other specific forms of noise include additive noise which occurs during image transmission over certain channels; multiplicative noise due to raster scan line degradation; and impulsive noise due to individual pixels of extremely bright or dark gray levels. The latter closely resembles sprinkled salt and pepper and therefore is also known as "salt and pepper noise."

For the removal of noise from IR images, several steps can be undertaken. The first and most important is that of frame averaging. This is normally accomplished by the camera itself where several incoming frames are averaged to reduce spikes and transmission noise. This limits, however, the frequency of sampling. Frame averaging can also be accomplished during digitization where multiple frames are acquired in memory and subsequently averaged to provide the final image.

Another common technique for suppressing noise[29, 32-33] is an operation known as smoothing. This procedure involves averaging intensity values of individual pixels in a specified image area. This averaging or mean filter operation involves replacing the intensity value of a pixel by the mean value of neighboring pixels in an NxN neighborhood. For simplicity, consider a 3x3 area where pixels are referred to as shown below

P_1	P_0	P_7
P_2	P_X	P_6
P_3	P_4	P_5

Here, the intensity value of central pixel P_X is replaced by the average of all nine pixels P_0 - P_7. The same process is applied to all pixels in the image to produce a

mean filtered image. The operation levels the effect of high intensity pixels represented in noise. However, mean filtering alone results in blurring of the edges or a smearing effect wherever there is sharp discontinuity in image intensity. Such loss in sharpness of the edges may be especially detrimental when one is interested in locating cracks or tracking a directional pattern of hot spots.

For IR images where there are sudden sharp transitions (spikes or impulses) present in the image, the preferred method for removing image noise is the median filter. In this method, the processing algorithm replaces the current pixel value with the median brightness of pixels in the neighborhood. In the 3x3 example given above, the brightness levels of 9 pixels are ranked in order, and the fifth (the median) value replaces the brightness level of the original central pixel. The idea being that median value is not affected by the noisy spikes in the intensity values of individual points. This approach has the advantage of preserving edges of the image with small, faint image parts remaining distinct. The technique can be applied iteratively with little blurring of the edges.

In practice, based on extensive prior experience with image analysis routines applied to such data, it is common to use a sequential or step approach to smoothing in order to eliminate noise. It is better to use combinations of a median and a mean or center-weighted mean filter to obtain a clearer portrait of temperature gradients in the image[28,32].

Image calibration follows the removal of noise where a calibration curve for the temperature range used by the equipment needs to be determined. The camera provides a gray bar outlining the correspondence between gray scale and temperature. The bar is used to extract the calibration curve and each image is then processed where the gray scales are adjusted so that their value represents temperature.

Following these steps, image analysis methods are required to derive pertinent data for temperature and its spatial distribution through the image. Numerical treatment of digital images allows construction of higher level interpretations through display of digital images as radiometric maps in relative or absolute radiant intensity of the object. Improved graphic depiction of temperature gradients is possible through temperature contour plots or isotherm maps[35].

Experimental Set-up for IR Thermography

This section describes a set of experiments using infrared imaging techniques for studying smoldering ignition in thin, porous materials such as cover fabrics used in upholstery construction. Figure 2 outlines the principal steps required for acquisition of thermal images and digital processing for extracting temperature distribution using IR thermography. Figure 3 depicts the instrumental set-up used in this study for making thermographic measurements using an IR thermal vision system. Upholstery fabric specimen (10x15 cm^2) held horizontally in the specimen holder was exposed to radiative energy from a glowing heater element for three minutes. The entire assembly was enclosed in a chamber with natural draft condition. The sample

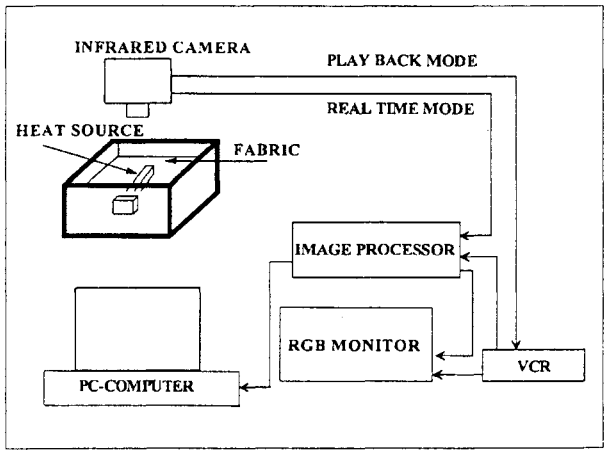

Figure 3. A Schematic of the Experimental Setup for Acquisition and Processing of Thermal Images.

holder was painted black using a high temperature, blackbody paint of high absorptivity to limit any reflective radiation from its surface to the object.
A radiant heating element or ignitor was selected to simulate a lit cigarette. After extensive search a commercial, diesel engine glow plug that is both of comparable dimensions and heat output to a lit cigarette was chosen. The ignitor (diameter 6 mm, heating element length 15 mm) was held parallel to and flush against the surface of the fabric. Output from the heating element was controlled using a variable power supply regulator. In this study, the ignitor was heated to yield a peak heat flux of 7.5 W/cm^2, corresponding to a range of peak heat output from the burning coal of high ignition propensity cigarettes examined in earlier studies[36].

The heat flux was measured with a Medtherm (model GTW 7-32-485A) Schmidt-Boelter heat flux gauge. The peak radiant heat output from the heating element was found to be consistent over a short term period up to 20 minutes. Although the approximate time for which the heating element is in contact with fabric surface is of the order of 2 minutes, the possibility that heat flux distribution incident on the fabric may change during this period was considered. This was assessed by axial scans of the heat output emitted along the length of the heating element. The gauge was mounted vertically on a positioning stand with the sensor facing the bottom of the heater element. Axial scans were carried out along the heater length (15 mm) varying the gauge position in 2 mm increments. The average peak value of the radiant flux (7.5 W/cm^2) was noted at the center of heater element. Radiometric maps of thermal images at one minute intervals were compared to test for sudden fluctuation in the temperatures across the heating element. No drastic shift in heat flux distribution was observed; the average peak flux varied by ±10 percent in the five trials that were conducted.

The IR thermal vision system comprises a commercial infrared scanner (Hughes Probeye 7300) and an image processor with an internal RGB monitor to provide a continuous image of the thermal scene. The system is connected to an external video monitor, a video cassette recorder, and a power supply charger. The IR camera views the target object at right angles and in close proximity to fill the instrument screen and minimize the effect of atmospheric attenuation. The IR scanner consists of a 30 element array of mercury cadmium telluride detectors with an electric cooling system. The IR scanner has a spectral range of 3.2-5.6 μm. Each image frame consists of 512x480 lines with a time resolution of 30 scans per second. The spatial resolution depends on the field of view selected. Each pixel corresponds to a square dimension of 0.625 mm on the target field surface.

The IR camera had been calibrated at a temperature of 600 ^{0}C. The calibration temperature is important because the output signal from IR camera corresponds to the temperature of the target field in terms of the difference between the radiation intensity of the unknown surface and that of a reference surface of known emissivity and temperature. If the IR device has been calibrated at a lower reference temperature, new calibration curves should be generated using a near blackbody material at temperatures comparable to that of the actual thermal scene.

Emissivity of the thermal scene is measured using a calibrated thermocouple (type K). The fabric surface temperature is not easy to measure. For this calibration, a fine thermocouple (0.05 mm, diameter) was inserted into the yarn at the top layer of the fabric. Approximately 3 mm length of thermocouple wire was inserted parallel to the fabric surface to ensure stable contact within the fabric. The surface temperature was measured at three different positions using the thermocouple and the emissivity setting on the IR instrument adjusted to obtain a temperature that matched

the thermocouple reading.

The entire heating process is video-recorded for later processing and extraction of temperature data. Video signals from the IR camera are recorded continuously until the ignitor causes the fabric to smolder in a self-sustained manner.

MATERIALS

The material chosen for this preliminary work was cotton duck, a densely woven fabric with a canvas-like construction. The firm construction of the fabric, due to the close packing of the yarns, results in an opaque material. Duck fabrics are made using plain weave construction in a range of areal density that spans from medium weight 270-340 g/m^2 (8-10 oz/yd^2) to a heavier construction 830 g/m^2 (24 oz/yd^2). These fabrics are made with 100 percent cotton fibers and generally available without any chemical finishing. Duck fabrics are required as the standard fabric in a test protocol developed by the National Institute of Standards and Technology (NIST) for a proposed standard test method to evaluate ignition propensity of cigarettes in an upholstered seating mockup[37]. The NIST study judged duck fabrics to be suitable for mockup ignition studies based on their uniform surface properties, reproducibility, smolder proclivity, and weight distribution representative of commercial upholstery cover fabrics. However much debate continues over the availability and validity of duck fabric as substitute for real, commercially representative test fabric for an ignition propensity test[38,39].

The physical properties of the two duck fabrics examined in this study are summarized in Table 1. Previous studies have confirmed the dominant influence of fabric weight (areal density) on ignition and burning rate. Both duck fabrics have similar chemical composition. Several studies have documented the presence and role of alkali metal ions, specifically the potassium and sodium cations, in affecting the smoldering propensity of cellulosic textiles[40-42]. The average potassium and sodium ionic contents of the two fabrics selected for this study were determined to be in the range of 5000-5500 parts per million, which is higher than the noted threshold level[41,42] above which cotton fabrics are certain to smolder.

RESULTS

Thermal images were digitized in gray scale where after calibration, each gray level corresponded to temperature. The first set of 10 images were obtained at 2 second intervals each, and subsequently image frames were captured at a 30 second interval. The images were calibrated to reflect true temperature values. This is because intensity values in the original image represent a specific temperature range, *i.e.*, from T_{min} to T_{max}. In this study, the temperature range was distributed over 250

Table 1: Properties of Duck Fabrics

Fabric Duck No.	Weight	Thickness	Wp Yn	Wf YN	WPC	FPC	Yarn Plies
	(g/m^2)	(mm)	(Nc)	(Nc)			
4	767.5	1/27	1.5	1/5	9.8	8.3	3
6	691.8	1.08	2.1	2.3	14.6	11	3
10	510.8	0.9	3.3	3.6	16.5	11.8	2

Nc: English cotton yarn size *WPC: Warp yarn per cm* *FPC: Filling yarn per cm*

degrees between 300 and 550 ^{0}C to correspond with 256 levels of gray.

Image processing routines are applied to edit and enhance images in order to derive the required information. Each image was first cropped to a suitable size representing the region of interest. This helps in saving disk storage space and loading time during processing. A median filter followed by a mean filter was applied to remove "noise" from the image. Figures 4–7 provide a contrast of the effectiveness of various smoothing operations for the removal of extraneous noise. The diagrams depict the respective effect of a mean and a median filter through the image of a smoldering wave and its corresponding *frequency distribution*, which gives the gray scale distribution of all the pixels. Figure 5 details the blurring effect due to average smoothing with the elimination of discontinuities, both around the edges and within the image of the smoldering char. This is because a mean filter (when used by itself) averages the intensity values of all the neighboring pixels including noise. In contrast, a median filter (Figure 6) retains any inflections of intensity values of pixels within the image, eliminating only those pixels with uncharacteristically high intensity values indicative of impulsive noise. A median filter is therefore more useful since the median value is generally associated with a real feature of the image, and very unlikely to be a noisy pixel.

A mean filter is used following median smoothing to obtain a clearer portrait of thermal gradients in the image. In this routine, a center weighted mean filter[30] is used. The combined effect of a median and a mean filter in succession is illustrated in Figure 7. The frequency data for each discrete intensity level can be used for the construction of a *cumulative distribution function* curve that gives the percentage of pixels above a specific gray level and which relates directly to temperature of corresponding points in the thermal scene.

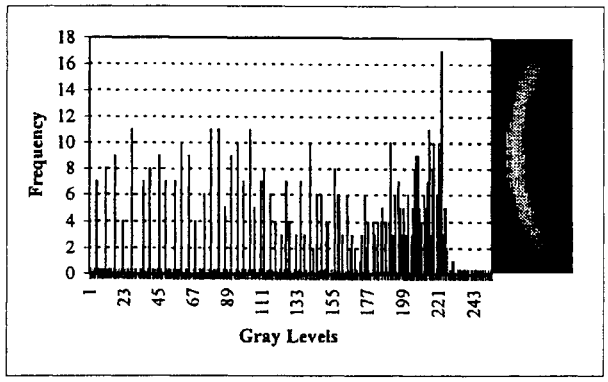

Figure 4. Original Image of the Smoldering Wave at 300 Seconds and the Frequency Distribution of Intensity Levels of Image Pixels.

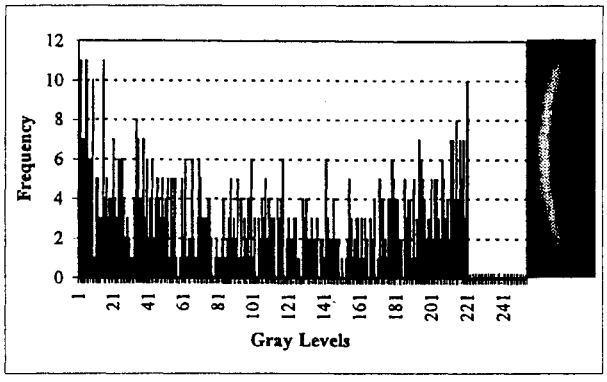

Figure 5. Mean Smoothing Filter-- showing Frequency Distribution of Intensity Levels of Pixels with the Removal of Noise and the Resultant Blurring of the Edges.

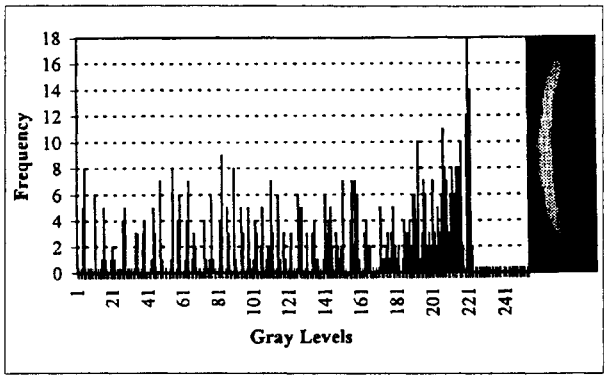

Figure 6. Median Smoothing Filter--Showing Frequency Distribution of Intensity Levels for the Image Processed with a Median Filter with Little Effect on Edges.

In the next step, temperature data were obtained from the statistical parameters of frequency distribution for each image frame. These parameters include the

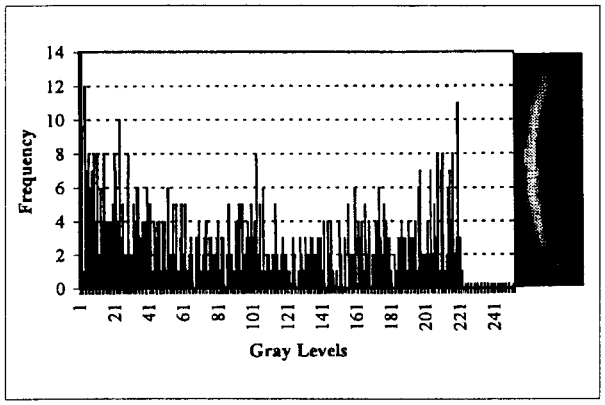

Figure 7. Median and Mean Filter -- Showing the Combined Effect of Two Filters on Frequency Distribution of Intensity Levels with the Removal of Impulsive Noise.

maximum and the minimum temperature points, mean and standard deviation, and pixel frequencies at specified percentile levels. The maximum temperature points at the fabric surface of both duck fabrics #6 (heavier) and #10 (lighter) are plotted in Figures 8 and 9; R1, R2 and R3 denote the three replicates for each fabric. It is clear that both fabrics undergo a rapid increase in temperature and start to smolder within one to two minutes of exposure. A steady temperature is maintained after the external heat source had been turned off. Temperature data for duck #10 show a consistent pattern among the three replicates with all traces converging together. However, data for duck #6 reveals a wider scatter in the temperature values, suggesting greater non-uniformities in the fabric properties. These non-uniformities result from variabilities in fabric and the constituent yarn structures and are more pronounced for coarser construction in case of duck #6 (Table 1). The exact manner in which these small constructional difference -- yarn fineness, twist and number of ply, fabric thickness, etc. -- are manifest in terms of char oxidation rate and the consequent energy feedback has not been determined.

Ohlemiller has enumerated the problems in defining the fabric ignition temperature and criteria for its measurement[36]. The ignition temperature of cotton, as determined by several researchers, lies between 400-450 ^{0}C. Visually, the smoldering ignition is marked by the appearance of the glowing char which starts to smolder away from the heating element, causing a hole in the specimen.

The ignition delay time, a function of imposed heat flux, is of the order of 8-10 seconds for duck #10 and 30 seconds for duck #6, the latter being the heavier-weight fabric. The low value of ignition delay time can be attributed primarily to the high heat flux emitted by the heating element. Also, the exothermic energy released due to oxidative pyrolysis of the cotton is much greater than any endothermic requirements for thermal degradation and heat losses from the surface. This results in a rapid increase of temperature, a thermal run away stage is reached, this stage is aided by the

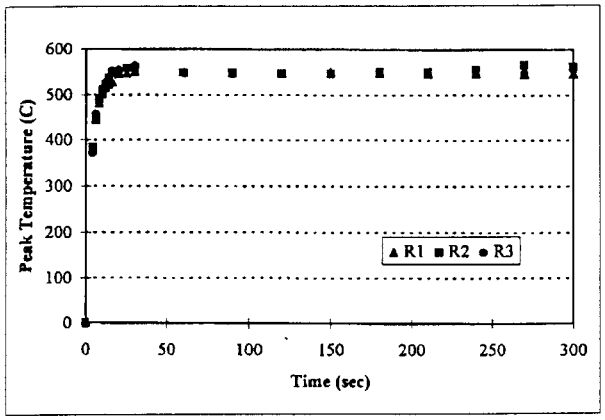

Figure 8. Maximum Surface Temperature as a Function of Time on Duck Fabric #10 Exposed to a Radiant Heat Flux of 7.5 W/cm^2.

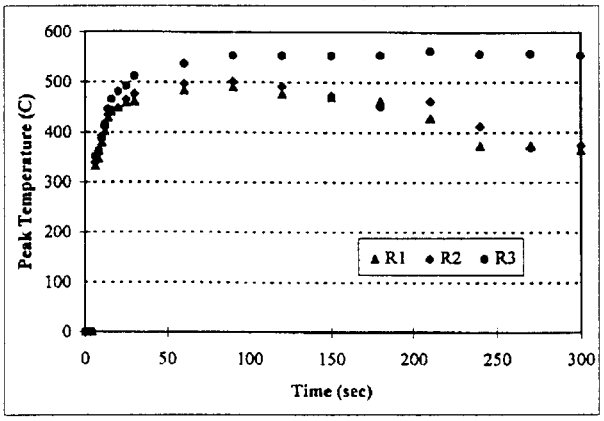

Figure 9. Maximum Surface Temperature as a Function of Time on Duck Fabric #6 Exposed to a Radiant Heat Flux of 7.5 W/cm^2.

absence of any heat sink (for example, foam padding) drawing heat away from the underside of the fabric. Under very simplistic conditions when the material is homogeneous and isotropic, with no change in thermophysical properties with temperature, the time to ignition is inversely related to fabric weight. Therefore, for comparative purposes, the difference in surface temperature and time to ignition between the two duck fabrics is indicative of the difference in fabric properties.

Figures 10 and 11 show the isotherm contours on the surface of the two fabrics at specified time intervals. The contour plots depict the surface temperature distribution on the duck fabrics at 90 sec (when the glowing char begins to recede away from the tip of the heating element), and at 330 sec (when the external heat source had been turned off). It was intended to observe if the cellulosic char would continue to oxidize with enough exothermic heat generation to continue smoldering in a self-sustained manner; and if possible to make an objective thermal comparison between the two materials with marginal differences in fabric properties.

The isotherm plots were obtained by a sequence of steps involving a profile trace of the intensity values along the pixel lines. Each linear profile trace gives the gray scale values (temperature) of each pixel point along that line. This step is repeated along the entire width of the thermal image to obtain a matrix of numbers representing the temperature values of all points in the region of interest. A surface plot of temperature values is obtained using this array of numbers which are easily converted to gray scale, or pseudo-colored temperature map, or isotherm contour plot of the kind shown in Figures 10 and 11. Areas under isotherm contours were calculated for these plots by counting the number of pixels within the corresponding image area. As noted earlier, the spatial resolution of each pixel in the selected field of view corresponds to a square dimension of 0.625 mm. Each pixel count was then converted to a surface isotherm area in square centimeters.

There are other techniques of creating such radiometric maps showing the gradient distribution of intensity values. By using image thresholding at multiple intensity (brightness) levels the image is converted to a binary form. All pixels above the specific brightness level are changed to white

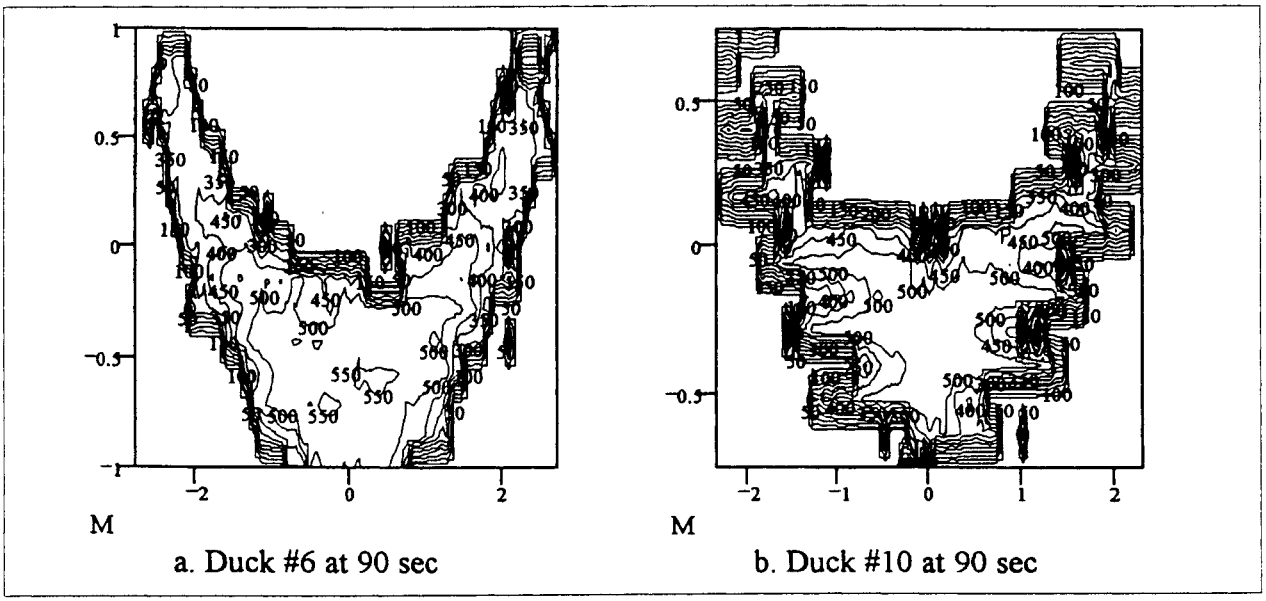

Figure 10. Surface Isotherm Contours of Various Temperatures at 90 Sec on a. Duck Fabric #6 and b. Duck Fabric #10.

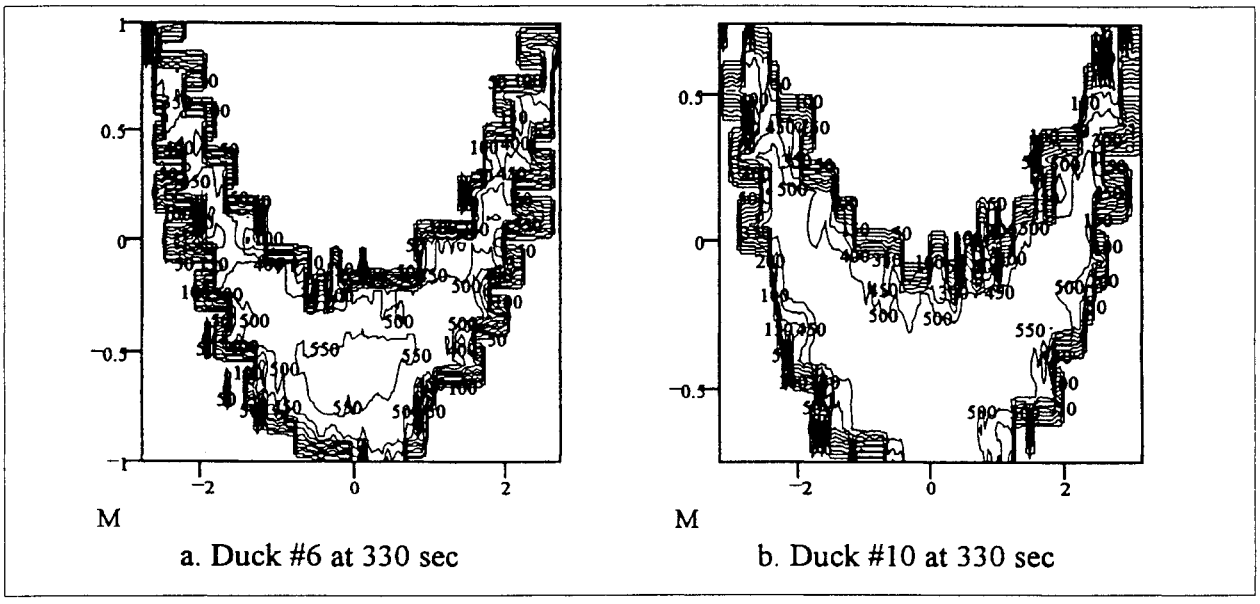

Figure 11. Surface Isotherm Contours of Various Temperatures at 330 Sec on a. Duck Fabric #6 and b. Duck Fabric #10.

(gray level 255) and those pixels below the threshold value changed to zero (black) producing a binary image and providing a spatial isotherm trace corresponding to the threshold intensity. These techniques however require some degree of *a priori* knowledge of brightness distribution in the image, and introduce some level of bias in the outcome[43].

Irregularity in the spatial distribution of the flux is apparent. This is due partly to the diffuse nature of the fabric surface which allows randomly distributed air pockets to control the oxidative reaction involving cellulosic char. An interesting feature that emerges from these plots is the difference in area within specific temperature isotherms. Areas under the 450 ^{0}C and 500 ^{0}C isotherms, given in the following section, were calculated for these plots.

Figures 10a and 10b depict the surface isotherm contours at 90 sec for fabric #6 and #10. The two duck fabrics show equal area enclosing the 450 and 500 ^{0}C isotherms. Cotton duck #6 depicted in Figure 10a has an area of 1.16 cm^2 and 0.76 cm^2 at 450 and 500 ^{0}C isotherms respectively. The lighter duck (Figure 10b) at same isotherms levels encloses an area 1.16 cm^2 and 0.73 cm^2. For both duck fabrics, the char area enclosing the 450 ^{0}C isotherm at 90 sec suggest that there is a certain volume of fabric that should attain a minimum temperature for smoldering ignition to occur, however the lighter duck #10 attains this temperature faster than does the heavier duck #6 (see Figures 8-9).

Figures 11a and 11b show the thermal contours on fabrics duck #6 and #10 respectively at 330 seconds; *i.e.*, absent any further external radiation as the ignitor was turned off at 300 sec. In both fabrics, the smolder wave continues to propagate with the aid of exothermic energy released via char oxidation. However, the comparison of isotherm area at 500 ^{0}C brings out a notable difference between the two fabrics. Lighter duck #10 (Figure 11b) has an area of 2.29 cm^2 compared to 1.5 cm^2 shown at duck #6, a difference of about 50 percent at same isotherm. An interesting feature of duck #6 (Figures 10a and 11a) is the presence of higher temperature still, obvious from the 550 ^{0}C isotherm areas. Further contour plots of these fabrics again reveal consistent differences between the isothermal areas at times up to 500 seconds.

CONCLUSIONS

A methodology has been presented for the determination of temperature field on the surface of porous textile material exposed to a low energy, localized heat source. A diesel glow plug or ignitor has been initially employed to simulate the behavior of a lit cigarette. Infrared thermography, coupled with PC-based image processing, allows measurement of dynamic changes in temperature distribution at the top surface of the exposed textile material. Measurement of correct emissivity of the thermal scene is critical for the accuracy of the temperature data derived through IR thermography, and precautions should be taken to prevent any ambient light reflection to the target surface.

In summary, infrared thermography is a useful technique for quantifying temperature profiles across the surface of a textile material. The system described here allows determination of the size and spatial geometry of isotherms that develop when a fabric is exposed to an external heat source. Measurement of temperature contours at various time intervals is helpful in establishing the correspondence between material properties and growth of conditions leading to smolder initiation. The isothermal patterns obtained with this technique are useful for discerning differences in burning characteristics of materials varying in physical and chemical properties.

A comprehensive set of experiments are underway using a new set of textile materials chosen to be representative of commercial upholstery fabrics. The experiments are designed to assess the effect of fabric physical and chemical properties on smolder ignition proclivity in the presence of a lit cigarette. The overall objective is to compare the measurement of temperature fields afforded by IR thermography, and to determine the smolder propensity and related combustion properties of textiles exposed to a low energy source. It is intended to demonstrate the efficacy of using a diesel glow plug to simulate a lit cigarette, and eventually to compare the resultant experimental data with theoretical predictions of the temperature fields and material properties.

In order to focus on smoldering behavior of fabrics and the effect of their properties, current experiments were conducted with a single fabric layer without any backing material. A future study is planned to include composite constructions with the fabric and an added layer of backing material such as foam padding.

ACKNOWLEDGMENTS

The authors appreciate the financial support for a portion of this study from the Society of Fire Protection Engineers Educational and Scientific Foundation. We wish to thank the Fire Protection and Sea Survival Branch of Naval Surface Warfare Center (NSWC), Annapolis, MD, for allowing the use of their facilities and other support and cooperation in conducting this work. We also thank the Cigarette Ignition Propensity Joint Venture Group for supplying the fabric samples used in this study. This research work is part of the overall requirements for the doctoral degree program of Sanjeev Gandhi at the University of Maryland.

Nomenclature

W	Radiant Energy, Watt/cm^2
E	Total Radiant Power, Watt
T	Temperature, K
I	Output Signal, Volts
A	Surface Area

Greek Letters

λ	Wavelength, μm
ε	Emissivity, dimensionless
ρ	Reflectance, dimensionless
τ	Transmittance, dimensionless
σ	Stefan-Boltzmann Constant, W/m^2•K^4

Subscripts

b Blackbody
n Net Radiation Flux
O Object
S Sensor

REFERENCES

1. Kasturi, R., and Trivedi, M.M., *Image Analysis Applications*, Marcel Dekker, New York, 1990.

2. Wu, Y., *Advanced Image Analysis Techniques for Identifying Carpet Appearance*, Doctoral Dissertation, University of Maryland, College Park, 1990, pp. 15-21.

3. Rao, P., *Application of Infrared Thermography for Quantitative Detection of Surface Flaws*, Masters Thesis, University of Maryland, College Park, 1989, pp. 21-23.

4. Milke, J.A. and Vizzini, A.J., "The Effects of Simulated Fire Exposure on Glass-Reinforced Thermoplastic Materials," *Journal of Fire Protection Engineering*, Vol. **5**, 1993, pp. 113-124.

5. Nicholas, J.V., and D.R. White, *Traceable Temperatures: An Introduction to Temperature Measurement and Calibration*, John Wiley & Sons, New York, 1994.

6. Bedrossian, J., "Industrial Applications of Fiber Optics in Infrared Thermal Monitoring," *Proceedings of International Society of Optical Engineers (SPIE)-An International Conference on Thermal Infrared Sensing for Diagnostics and Control (Thermosense IX)*, Orlando, Florida, 18-20 May, 1987, Vol. **780**, pp. 90-96.

7. Hughett, P., "Image Processing Software for Real Time Quantitative Infrared Thermography," *Proceedings of SPIE-An International Conference on Thermal Infrared Sensing for Diagnostics and Control (Thermosense IX)*, Orlando, Florida, 18-20 May, 1987, Vol. **780**, pp. 176-183.

8. Lloyd, J.M., *Thermal Imaging Systems*, Plenum Press, NY, 1975, pp. 7-15.

9. Ahlstrom, J., "Review of Industrial and Research Applications of Thermography," *Proceedings of SPIE Conference-Infrared Technology and Applications*, London, England, 26-28 June, 1990, Vol. **1320**, pp. 292-294.

10. Chang, Y.M., "An Investigation into Factors Affecting Infrared Temperature Measurements for Building Applications," *Proceedings of SPIE-An International Conference on Thermal Infrared Sensing for Diagnostics and Control (Thermosense IX)*, Orlando, Florida, 18-20 May, 1987, Vol. **780**, pp. 11-16.

11. Lyberg, M.D., Mattson, M. and Sundberg, J., "Detection of Moisture Damage in Buildings Using Thermography," *Proceedings of SPIE-An International Conference on Thermal Sensing and Imaging Diagnostic applications (Thermosense XII)*, Orlando, Florida, 18-20 April, 1990, Vol. **1313**, pp. 100-105.

12. Williams, V.H. and Fike, D.K., "Failure Analysis of Raw Printed Circuit Boards Using IR Thermography," *Proceedings of SPIE-An International Conference on Thermal Infrared Sensing for Diagnostics and Control (Thermosense IX)*, Orlando, Florida, 18-20 May, 1987, Vol. **780**, pp. 231-235.

13. Clark, R.P. and Goff, M.R., "Medical Thermography: Current Status," *Proceedings of SPIE-Infrared Technology and Applications*, London, England, 26-28 June, 1990, Vol. **1320**, pp. 242-250.

14. Schleimann-Jansen, A., and Forsberg, K., "New Test Method for Determination of Emissivity and Reflection Properties of Protective Materials Exposed to Radiant Heat," *Performance of Protective Clothing, ASTM STP 900*, American Society for Testing and Materials, Philadelphia, PA, 1986, pp. 376-386.

15. Hayasaka, H., Koseki, H., and Tashiro, Y., "Radiation Measurements in Large-Scale Kerosene Pool Flames Using High-Speed Thermography," *Fire Technology*, Vol. **28**, No. 2, 1992, pp. 110-122.

16. Arakawa, A., Saito, K., and Gruver, W.A., "Automated Infrared Imaging Temperature Measurement," *Study of Fire Induced Flow Along the Vertical Corner Wall, Part 2*, National Institute of Standards and Technology, NIST-GCR-93-628, 1993, pp. 1-12.

17. Zissis, G.J., "Fundamentals of Infrared - A Review," *Proceedings of SPIE-Modern Utilization of Infrared Technology - Civil and Military*, San Diego, California, 19-20 August 1975, Vol. **62**, pp. 67-95.

18. Noltingk, B.E., ed., "Measurement of Temperature and Chemical Composition," *Instrument Technology*, Butterworths, Boston, Vol. **3**, 1985, pp. 92-94.

19. Hudson, R.D., *Infrared System Engineering*, Wiley Interscience, John Wiley and Sons, New York, 1969, pp. 20-45.

20. Beers, W.A., "Cooling Hot Spots With Thermography," *Proceedings of the Third Biennial Infrared Information Exchange (IRIE)*, St. Louis, Missouri, 24-26 August, 1976, pp. 1-4.

21. Fraden, J., *AIP Handbook of Modern Sensors: Physics, Designs and Applications*, Modern Instrumentation and Measurements in Physics and Engineering, American Institute of Physics, New York, 1993.

22. Braumberg, G.C., *Computer Aided Infrared Thermography Using Emissivity Compensated Imaging*, Masters Thesis, University of Maryland, College Park, 1990.

23. Klassen, M. and Di Marzo, M., "Infrared Thermography of Dropwise Evaporative Cooling," *Experimental Thermal and Fluid Science*, Vol. **5**, 1992, pp. 136-141.

24. Pratt, W.K., *Digital Image Processing*, John Wiley & Sons, New York, 1978.

25. Bret, M., *Image Synthesis*, Kluwer Academic Publishers, Boston, 1992.

26. May, T.H., Stamm, G.L., and Blodgett, J.A., "Applications of Digital Processing to Calibrated Infrared Imagery," *Proceedings of SPIE-Infrared Systems*, Huntsville, Alabama, 30 September - 1 October, Vol. **256**, 1980, pp. 55-61.

27. Green, W.B., *Digital Image Processing: A Systems Approach*, Van Nostrand Reinhold, New York, 1983 pp. 14-27.

28. Wu, Y., Pourdeyhimi, B., and Spivak, S.M., "Texture and Appearance Measurement of Carpets Using Image Analysis," *Textile Research Journal*, Vol. **61**, No. 7, 1991, pp. 407-419.

29. Sonka, M., Hlavac, V., and Boyle, R., *Image Processing, Analysis and Machine Vision*, Chapman & Hall, New York, 1993, pp. 13-106.

30. Gonzalez, R.C. and Wintz, P., *Digital Image Processing*, Addison-Wesley, Reading, Massachusetts, 1987, pp. 139-175.

31. Dawson, B.M., "Introduction to Image Processing Algorithms," *BYTE*, Vol. **12**, No. 3, 1987, pp. 169-187.

32. Milgram, D.L. and Rosenfeld, A., "Object Detection in Infrared Images," *Digital Image Processing*, Lecture Notes in Computer Science, Springer-Verlag, New York, 1981, pp. 228-353.

33. Foith, J.P., Eisenbarth, C., Enderle, E., Geisselmann, H., Ringshauser, H., and Zimmermann, G., "Real-Time Processing of Binary Images for Industrial Applications," *Digital Image Processing*, Lecture Notes in Computer Science, Springer-Verlag, New York, 1981, pp. 61-168.

34. Mao, Z. and Strickland, R.N., "Image Sequence Processing for Target Estimation in Forward Looking IR Imagery," *Image Processing, Analysis, Measurement, and Quality, Proceedings of SPIE*, Los Angles, California, 13-15 January, Vol. **901**, 1988, pp. 44-53.

35. Pourdeyhimi, B., Ulcay, Y., Ramanathan, R., and Sobus, J., "Measuring Heat of Polymerization in Acrylic Bone Cements Using Infrared Thermographs," *Proceedings of the 16th Annual Energy-Sources Technology Conference and Exhibition,* Houston, Texas, Vol. **53**, 1993, pp. 259-262.

36. Gann, R.G., Harris, R.H., Krasny, J.F., Levine, R.S., Mitler, H.E., and Ohlemiller, T.J., *The Effect of Cigarette Characteristics on the Ignition of Soft Furnishings*, NBS Technical Note 1241, 1988, pp. 105-135.

37. Ohlemiller, T.J., Villa, K.M., Braun, E., Eberhardt, K.R., Harris, R. H., Lawson, J.R., and Gann, R.G., *Test Methods for Quantifying the Propensity of Cigarettes to Ignite Soft Furnishings*, NIST Special Publication 851, 1993, pp. 7-20.

38. Jupe, R., Shipley. D.K., Hudson, W.Z., Wanna, J.T., and Greear, L.C., "Inter-Bolt Variability of Cotton Duck #4 and the Effects on Cigarette Ignition Propensity Test Outcome," *Journal of Fire Sciences*, Vol. **13**, 1995, pp. 127-140.

39. Lewis, S.L., Morton, M.J., Norman, V., Ihrig, A.M., and Rhyne, A.L., "The Effects of Upholstery Fabric Properties on Fabric Ignitabilities by Smoldering Cigarettes, II," *Journal of Fire Sciences*, Vol. **13**, 1995, pp. 445-471.

40. Ihrig, A.M., Rhyne, A.L., Norman, V., and Spears, A.W., "Factors Involved in the Ignition of Cellulosic Upholstery Fabrics by Cigarettes," *Journal of Fire Sciences*, Vol. **4**, 1986, pp. 237.

41. McCarter, R.J., "Smoldering Combustion of Cotton and Rayon," *Journal of Consumer Product Flammability*, Vol. **9**, 1977, pp. 31-34.

42. Ihrig, A.M., Smith, S., "The Role of Alkali and Alkaline Earth Metal Ions in Cellulosic Smoldering," *Journal of Fire Sciences*, Vol. **12**, 1994, pp. 357-365.

43. Russ, J.C., *Computer-Assisted Microscopy--The Measurement and Analysis of Images*, Plenum Press, New York, 1990.